Catalysis Letters Vol. 99, Nos. 3–4, February 2005 (© 2005)
DOI: 10.1007/s10562-005-2106-8

Oxidative property of Nb-containing MCM-41 molecular sieves for vapor phase oxidation of *m*-toluidine

S. Vetrivel and A. Pandurangan*

Department of Chemistry, Anna university, Chennai-600 025, India

Received 9 July 2004; accepted 15 October 2004

Mesoporous Nb-MCM-41 molecular sieves (Si/Nb = 50 and 75) were synthesized hydrothermally. As-synthesized and calcined catalysts were characterized by low angle X-ray powder diffraction (XRD), N_2-adsorption isotherm, thermogravimetric and FT-IR techniques. The niobium impregnated MCM-41 catalysts were also prepared by wet method and their structure was elucidated XRD and FT-IR spectroscopy. Electron spinning resonance (ESR) studies conformed the co-ordination environment of niobium in both type of catalysts. The catalytic activity of the above catalysts was studied for the vapor phase oxidation of *m*-toluidine with CO_2-free air at 200, 250, 300, 350, 400 °C. The major products were *m*-aminobenzoic acid and *m*-aminobenzaldehyde. The *m*-toluidine conversion was found to be higher in niobium impregnated catalysts than incorporated catalysts. The selectivity to *m*-aminobenzoic acid, which was the principally aimed product in this study, was found to be higher than that of the *m*-aminobenzaldehyde. The activities of catalysts follow the order Nb-MCM-41 (1%) > Nb-MCM-41 (2%) > Nb-MCM-41 (3%) > Nb-MCM-41 (50) > Nb-MCM-41 (75). The effect of weight hourly space velocity and time on stream was also studied on conversion and products selectivity and the results are discussed. Conditions were optimized for better *m*-toluidine conversion and products selectivity.

KEY WORDS: synthesis; Nb-MCM-41; air oxidation; *m*-toluidine; *m*-aminobenzoic acid.

1. Introduction

The oxidation of organic substrates lead to the production of many functionalized molecules which are of great commercial and synthetic importance. The oxidizing agent such as peroxyacids and peroxides is widely used but suffers from the hazardous nature of the reagent and the by-products produced [1]. The dominant position of molecular oxygen as the oxidant for bulk chemical oxy-functionalizations is due to the fact that it is the only economically and environmentally friendly feasible oxidant for large-scale processing. The oxidation of hydrocarbons catalyzed by transition metal complexes has been studied extensively [2–5]. In this study, the high temperature oxidation of *m*-toluidine with molecular oxygen over the niobium containing mesoporous molecular sieves were carried out and discussed. The oxidation product namely *m*-aminobenzoic acid and used in the production of dyes and pesticides. It is also an intermediate in organic synthesis.

In the case of MCM-41 molecular sieves, active sites may be generated by the incorporation of heteroatom into the electrically neutral purely siliceous framework. Various elements have already been introduced into the MCM-41 framework, for example:aluminium [6–8], gallium [9], titanium [10,11], vanadium [12], iron [13], manganese [14,15] and chromium [16]. The incorporation of niobium into the MCM-41 framework material was reported by Maria *et al.* [17] for the first time. Niobium containing catalysts can exhibit a large variety of catalytic activities depending on the localization of the niobium element and its surroundings. In catalysis, niobium compounds can play various functions, as follows:promoter or active phase, support, solid acid catalyst or redox materials [18]. In this paper, the mesoporous molecular sieves of MCM-41 type containing niobium mainly in the framework and niobium impregnated forms are studied. The structural and textural properties of the synthesized catalysts have been characterized by employing various physico-chemical techniques. The catalytic activity of all the catalysts was evaluated in oxidation of *m*-toluidine with air. The conversion and products selectivity of the reaction such as reaction temperature, weight hourly space velocity, and time on stream were studied and the results discussed.

*To whom correspondence should be addressed.
E-mail: pandurangan_a@yahoo.com

2. Experimental

2.1. Synthesis catalysts

Niobium incorporated MCM-41 (Si/Nb = 50 and 75) samples were synthesized hydrothermally. Sodium metasilicate (E-Merck) and niobium pentachloride (E-Merck) were used as the sources for silicon and niobium, respectively. Cetyltrimethylammonium bromide (CTAB) (E-Merck) was used as the structure-directing agent. In a typical synthesis, 21.2 g of sodium metasilicate dissolved in 80 ml deionized water was mixed with appropriate

amount of niobium pentachloride (dissolved in 25 ml alcohol). This mixture was stirred for 1 h using a mechanical stirrer and the pH of the solution was adjusted to 10.5 with continuous stirring to form a gel. After that, an aqueous solution of CTAB was added dropwise (25 m1/h) through the syringe infusion pump so that the gel was changed into suspension. The molar composition of the resultant mixture was $SiO_2 : xNbCl_5 : 0.2CTAB : 0.89H_2SO_4 : 120H_2O$ (x varies with Si/Nb ratio). The suspension was transferred into a Teflon-lined steel autoclave and heated to 120 °C for 2 days. After cooling to room temperature, the product formed was filtered, washed with deionized water and finally calcined at 550 °C for 6 h in flowing air.

Si-MCM-41 was also synthesized in a similar manner wherein only without the addition of niobium pentachloride.

2.2. Preparation of impregnated catalysts

1, 2 and 3 wt% niobium pentachloride solution was prepared and mixed with 3 g of Si-MCM-41 catalyst to prepare 1, 2 and 3% niobium impregnated catalysts respectively, by stirring for 6 h. The residue was filtered and washed in deionized water and alcohol in order to remove any ions adsorbed on the external surface. The filtrate was dried under reduced pressure, and finally calcined in air at 550 °C for 6 h.

2.3. Physico-chemical characterization

The structure of the niobium containing MCM-41 molecular sieves was analyzed by low angle X-ray powder diffraction (XRD) on a Siemens D5005 stereoscan diffractometer equipped with liquid nitrogen-cooled germanium solid-state detector using Cu Kα radiation. ASAP-2010 volumetric adsorption analyzer manufactured by the Micromeritics Corporation (Norcross, GA) was used to determine the specific surface area of the catalytic samples at liquid nitrogen temperature. Before the nitrogen adsorption–desorption measurement, each sample was degassed at 623 K at 10^{-5} Torr overnight in an out-gassing station of the adsorption apparatus. The full adsorption–desorption isotherm was obtained using BET method at various relative pressures; the pore size distribution and wall thickness were calculated from the nitrogen adsorption–desorption isotherms using the BJH algorithm (ASAP 2010 built in software from Micromeritics). The catalysts were characterized by FT-IR spectroscopy in a Nicolet (Avatar 360) spectrometer using potassium bromide (KBr) pellet technique. The spectra were recorded at room temperature in the region of 400–4000 cm^{-1}. Thermal decomposition of the as-synthesized samples was examined on Rheometric scientific (STA 15 H^+) thermobalance. 10–15 mg of as-synthesized MCM-41 sample was placed in a platinum pan and heated from 30 to 1000 °C at a heating rate of 20 K min^{-1} in air with a flow rate of 50 ml/h. The spectra were recorded in air at room temperature. The co-ordination environment of all the catalysts was analyzed by ESR technique (Varian E112 spectrometer operating in the X-band 9-GHz region). DPPH was used as the reference to mark the g-value. The relative ESR intensities were calculated by double integration of the recorded ESR signal. The size and morphology of Si-MCM-41 and Nb-MCM-41 (50) samples were recorded using a JEOL 640 scanning electron microscope (SEM) operating at an accelerating voltage of 10 kV. Samples were mounted using a conductive carbon double-sided sticky tape. The samples were sputtered with gold (ca. 10 nm) to reduce the effect of charging.

2.4. Catalytic studies

The oxidation of *m*-toluidine with CO_2-free air was carried out in a fixed bed down flow quartz reactor under atmospheric pressure in the temperature range of 200–400 °C in steps of 50 °C. Prior to the reaction, the reactor packed with 0.3 g of the catalyst sample was preheated in a tubular furnace equipped with a thermocouple. The *m*-toluidine was fed into the reactor using a syringe infusion pump at a predetermined flow rate. The oxidation of *m*-toluidine was carried out and the products mixture was collected for a time interval of 1 h. The products were analyzed by gas chromatography (Hewlett-Packard 5890A) equipped with Flame Ionization Detector and PONA column. The identification of products was also performed on a Shimadzu GC-MS-QP 1000EX gas chromatograph-mass spectrometer. No significant *m*-toluidine conversion was observed when the reaction was carried out without catalyst indicating that there is no thermal effect on conversion.

All the catalysts were regenerated by burning a way the coke deposit formed by passing air at a temperature of 500 °C for 6 h. The catalysts were used continuously to study the effect of various parameters, viz., temperature, weight hourly space velocity and time on stream.

3. Results and discussion

3.1. X-ray diffraction

The powder XRD patterns of niobium incorporated and impregnated MCM-41 catalysts are shown in figures 1**a–c**. It can be observed that all the above materials exhibit a strong peak in the 2θ range 1.9–2.4°. Additionally two broad peaks at 2θ range 3.5–4.5° indicating the formation of well-ordered mesoporous materials. The d_{100} values and unit cell parameters of the mesostructured materials are listed table 1. The differences in intensity of the reflections are not highly significant. Marler *et al.* [19] have shown that the

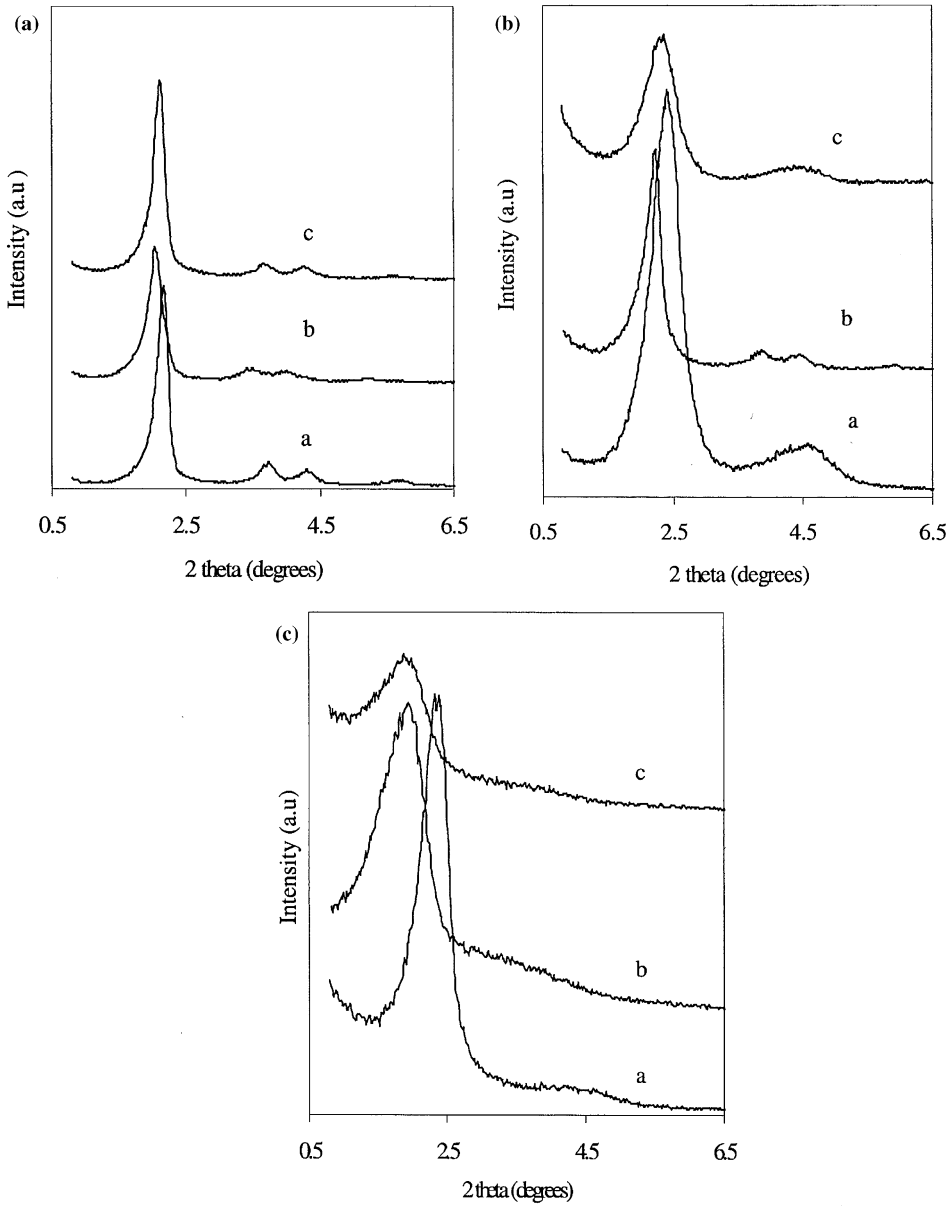

Figure 1. XRD of **(a)** as-synthesized, **(b)** Calcined (a) Si-MCM-41, (b) Nb-MCM-41 (50), (c) Nb-MCM-41 (75) and **(c)** after impregnation (a) Nb-MCM-41 (1%), (b) Nb-MCM-41 (2%), (c) Nb-MCM-41 (3%).

intensities of the XRD peaks are related to the difference in scattering power between the amorphous silica wall and the in-pore amorphous organic phase. The hexagonal unit cell parameter (a_0) was calculated using the formula $a_0 = 2d_{100}/\sqrt{3}$, which was obtained from the peak in the XRD pattern by Bragg's equation ($2d \sin\theta = \lambda$, where $\lambda = 1.54$ Å for the Cu Kα radiation). The value of a_0 is equal to the internal pore diameter plus one pore wall thickness [20]. Further, the appearance of the above peaks in Nb-MCM-41 catalysts suggested that the hexagonal array of mesopores in MCM-41 was sustained after the incorporation of metal in the framework. Table 1 shows that the d_{100} spacing and unit cell parameters of niobium containing samples were larger than siliceous MCM-41 and increased with increasing niobium content.

The contraction of the hexagonal unit cell parameter after calcination is very small, and the d_{100} distance was reduced, suggesting a high thermal stability. It is noted that two groups of overlapping diffraction peaks can be observed in the samples after calcination. As-synthesized MCM-41 gave a quality XRD pattern (figure 1**a)** with sharp peaks than that of calcined MCM-41 samples. After calcination to decompose the surfactant, the XRD patterns of MCM-41 become broader peaks (figure 1**b**). The intensity of 100 reflections was decreased and the 2θ positions shift to a higher value indicating a contraction of the lattice caused by template

Table 1
Structure parameters for the Nb-containing MCM-41 molecular sieves

Catalysts	As-synthesized		Calcined		Contraction	After impregnation		g-value of ESR
	d_{100} (Å)	a_0 (Å)	d_{100} (Å)	a_0 (Å)		d_{100} (Å)	a_0 (Å)	
Si-MCM-41	40.49	46.75	34.63	39.99	6.76	–	–	–
Nb-MCM-41 (50)	43.27	49.96	39.41	45.51	4.45	–	–	2.0241
Nb-MCM-41 (75)	41.25	47.63	37.40	43.19	4.44	–	–	2.0125
Nb-MCM-41 (1%)	–	–	–	–	–	37.09	42.83	2.2743
Nb-MCM-41 (2%)	–	–	–	–	–	45.04	52.01	2.2778
Nb-MCM-41 (3%)	–	–	–	–	–	44.58	51.48	2.2635

removal and subsequent condensation of silanol groups. The XRD patterns of the after impregnated samples (figure 1**c**) shows that the intensity of the patterns due to 100 plane was decreased and that of 110 and 200 planes disappeared owing to radiation diffusion. This can be attributed to the nanosites of impregnated particles present in the pores.

3.2. BET surface area

The nitrogen adsorption isotherms of the calcined Si-MCM-41 and Nb-MCM-41 (50) samples exhibited the sharp characteristic of mesoporous materials with regularly sized pores. The adsorption isotherms of these catalysts are presented in figures 2**a** and **b**. The monolayer adsorption on the walls of the mesopores is responsible for the nitrogen uptake at low relative pressures ($P/P_0 < 0.3$). A sharp steep at intermediate P/P_0 may indicate the capillary condensation in the mesopores and a plateau portion at high P/P_0 associated with multilayer adsorption on the external surface of the materials. Both the catalysts show a characteristic step around $P/P_0 \approx 0.3$ indicating the mesoporous nature of the materials [21]. The sharpness and height of the capillary condensation step are the indications of pore size uniformity. Deviation from sharp and well-defined pore filling step are the indication of increase in pore size heterogeneity. From the plot of the pore-size distribution, we can see a well-defined pore size distribution centered around 32 Å. The pore size distribution curves of the Nb-MCM-41 show a slight increase in their half-height width of the peak at around 32 Å if compared with that of the Si-MCM-41 sample. It indicates that the mesoporosity was somewhat degraded after incorporation of the niobium metal. The pore size distribution of these mesoporous materials, their corresponding BET surface area and the cumulative BJH desorption pore volumes are listed in table 2. It indicates that the niobium containing samples have thicker pore walls, larger distances between pore centers and larger surface area than the siliceous MCM-41. It can be seen that, upon introducing the niobium metal into the mesoporous MCM-41, the pore size increase.

3.3. FT-IR spectroscopy

The FT-IR spectra of as-synthesized Si-MCM-41, Nb-MCM-41 (50) and Nb-MCM-41 (75) are shown in figure 3**a**. The broad band around 3500 cm^{-1} is due to O–H stretch of water and silanol defects. The less intense peaks in the spectra of as-synthesized samples around 2920 and 2960 cm^{-1} are due to symmetric C–H and asymmetric CH_2 vibrations of the surfactant molecules. Their corresponding peak between 1500–1670 cm^{-1} is due to OH_2 bend. The peak between 500 and 1200 cm^{-1} are assigned to framework vibrations. The intense peak at 1120 cm^{-1} is attributed to the asymmetric stretching of T–O–T groups. The symmetric

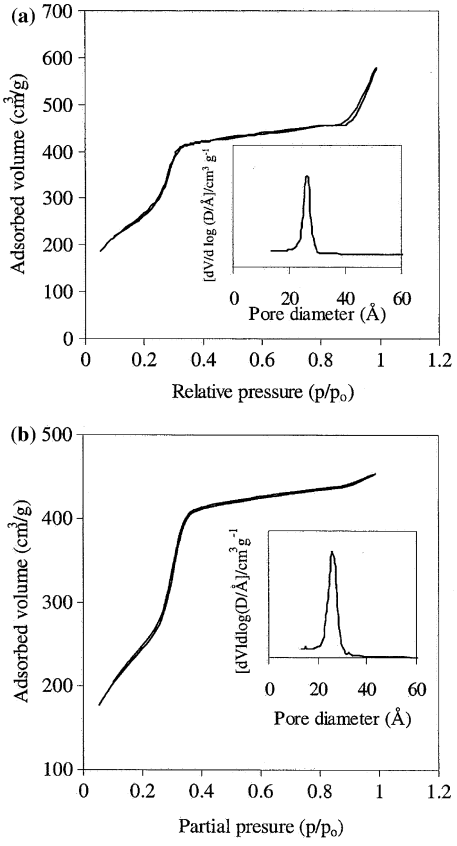

Figure 2. N_2 adsorption isotherm of calcined **(a)** Si-MCM-41 and **(b)** Nb-MCM-41 (50).

Table 2
Physico-chemical characterization of Si-MCM-41 and Nb-MCM41 catalysts

Catalysts	N_2-adsorption isotherm				TG-DTA weight loss (wt%)			
	BET surface area (m^2 g^{-1})	Pore size (Å)	Pore volume (cm^3 g^{-1})	Wall thickness (Å)	Total	50–150 °C	150–350 °C	350–550 °C
Si-MCM-41	949	30.1	0.95	16.65	52.36	11.43	32.49	8.4
Nb-MCM-41 (50)	978	32.7	0.97	17.26	41.88	7.50	25.28	9.1
Nb-MCM-41 (75)	–	–	–	–	43.66	10.02	26.84	6.8

stretching modes of T–O–T groups are observed around 864 cm^{-1}, and the peak at 476 cm^{-1} is due to the bending mode of T–O–T. The peak at 960 cm^{-1} is assigned to the presence of Si–O vibrational mode perturbed by the presence of metal ions in a neighboring position [22]. Some authors use this band for evidence of the incorporation of metal into the siliceous framework (Si–O–T) [23,24]. The FT-IR spectra of the calcined and impregnated samples are shown in figure 3**b** (a–f). The absence of peaks at 2920 and 2960 cm^{-1} illustrate complete expulsion of the template. The bands at 3500 and 1670 cm^{-1} in figure 3**a** are also completely absent in figure 3b (a, b and c).

3.4. TG-DTA study

Thermogravimetric and differential thermalanalysis of the Si-MCM-41 and Nb-MCM-41 catalysts are given in figure 4. The thermal patterns of the three samples are qualitatively very similar. The total weight losses are 52.36, 41.88 and 43.66 wt% for samples Si-MCM-41, Nb-MCM-41 (50) and Nb-MCM-41 (75), respectively. The weight loss was increased when niobium content was lower (table 2); this clearly demonstrates that a larger amount of niobium is planted on the channel surface in Nb-MCM-41 (50) than in Nb-MCM-41 (75). The TGA patterns have at least three distinct stages of weight loss. A first weight loss due to the desorption of water amounting (~11.43–10.02%) was observed between 50 and 150 °C corresponds to the desorption and removal of the water molecules physisorbed on the external surface of the crystallites or occluded in the macropores and mesopores present between the crystallite aggregates. The second stage of 150–350 °C, corresponding to a weight loss of (~32.49–26.84%) can be ascribed to the decomposition of the surfactant species.

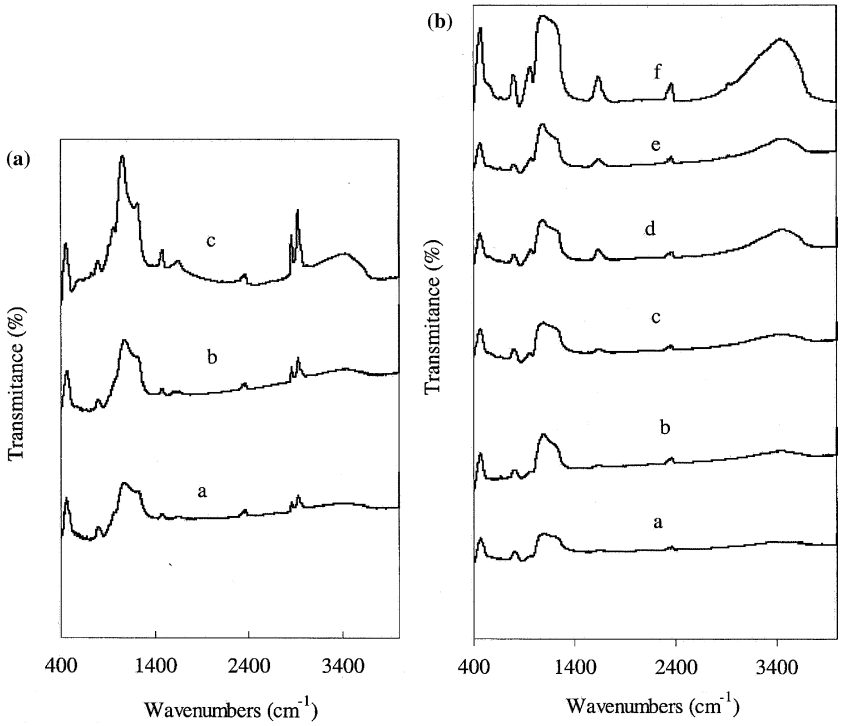

Figure 3. FT-IR spectra of **(a)** as-synthesized (a) Si-MCM-41, (b) Nb-MCM-41 (50), (c) Nb-MCM-41 (75) and **(b)** calcined (a) Si-MCM-41, (b) Nb-MCM-41 (50), (c) Nb-MCM-41 (75) and after impregnation (d) Nb-MCM-41 (1%), (e) Nb-MCM-41 (2%), (f) Nb-MCM-41 (3%).

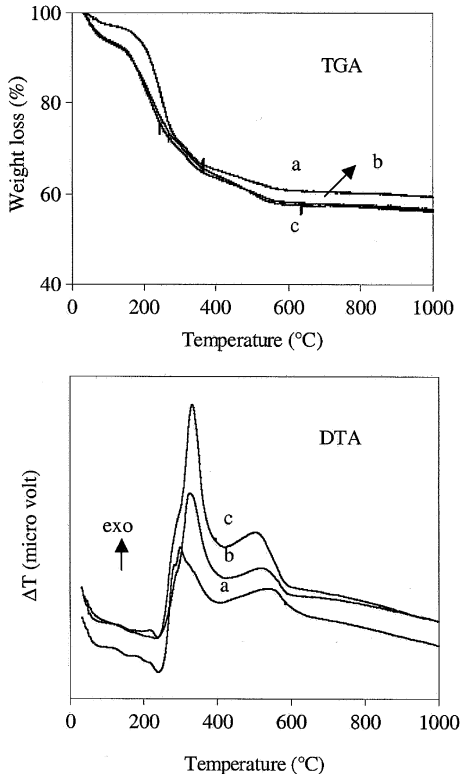

Figure 4. TG-DTA curve of as-synthesized (a) Si-MCM-41, (b) Nb-MCM-41 (50), (c) Nb-MCM-41 (75).

Finally, the weight loss of (~8.44–6.8%) from 350 to 550 °C can be assigned to water loss from the condensation of adjacent silanol groups to form a siloxane bond.

Thermogravimetric analysis in combination with XRD peaks showed that samples were thermally-stable at calcination conditions. The organic template was decomposed below 550 °C, the weight loss for all of the samples was in the range of about 40–52 wt%, which indicated that as-synthesized samples contained large amounts of organic templates because of the presence of mesoporous materials with large void volume [25]. The DTA curves are shown in the figure 4. All the curves in the broad exotherm between 200 and 550 °C coincide with the weight loss in the TGA traces between 200 and 550 °C. Hence, it is ascribed to loss of oxidative decomposition of template. Above 550 °C, there is neither exothermic nor endothermic peak illustrating the materials are stable up to 1000 °C.

3.5. ESR spectroscopy

In the ESR spectra of niobium incorporated and impregnated mesoporous molecular sieves there is evidence for paramagnetic centers. The ESR spectra due to impregnated samples (figures 5a–c) shows characteristics signal corresponding to Nb^{4+} ($g = 2.2$) [26]. The first three spectra appear nearly similar suggesting similar environment for Nb^{4+} irrespective of the level of

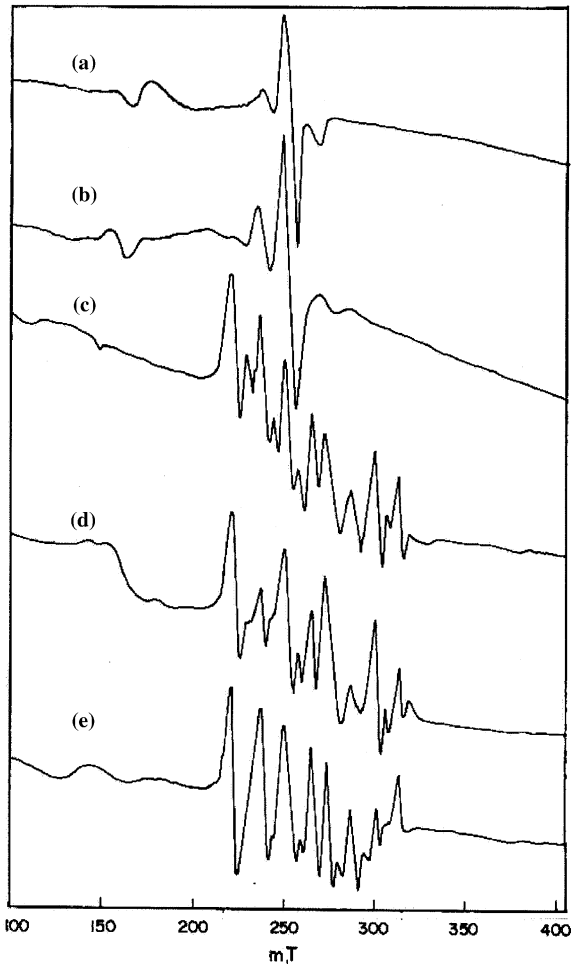

Figure 5. ESR spectra of calcined (a) Nb-MCM-41 (1%), (b) Nb-MCM-41 (2%), (c) Nb-MCM-41 (3%), (d) Nb-MCM-41 (50), (e) Nb-MCM-41 (75).

impregnation. In figures 5d and e, there are no ESR signal characteristic of Nb^{4+} hence the presence of Nb^{4+} either in the framework or in the non-framework is completely ruled out. Nb^{5+} cannot give ESR signal. But the samples give rise to signal with $g = 2.0$. These two spectra appear very much close to those observed by Maria *et al.* [18]. They reported that the signal was due to dehydroxylation (shown below) of penta co-ordinated niobium leading to the formation of $Nb\text{-}O^{-}$ species. Actually a hole is mainly localized on an oxygen atom and near a niobium atom [27,28]. It was also ascribed to carbon radicals formed from residual traces of template [29].

3.6. Scanning electron microscopy (SEM)

The size and morphology of Si-MCM-41 and Nb-MCM-41 (50) were investigated by SEM. The SEM images of these catalysts are shown in figures 6a and b. It seemed that the samples do not have well-defined structure. Further, aggregates without regular shapes are observed, it indicating a slight reduction in hexagonal

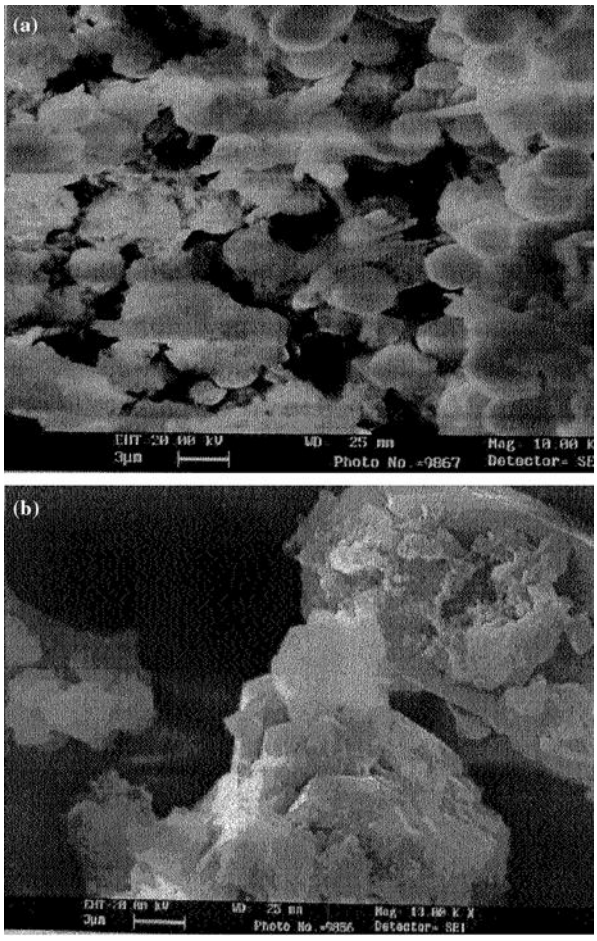

Figure 6. SEM pictures have (a) Si-MCM-41 and (b) Nb-MCM-41 (50).

symmetry of MCM-41 due to metal incorporation. In figure 6b, the morphologies were lots of stepped and smooth jagged crystals aggregating and packing randomly.

3.7. Effect of temperature

Vapor phase *m*-toluidine oxidation was carried out in air over Nb-MCM-41 (1%), Nb-MCM-41 (2%), Nb-MCM-41 (3%), Nb-MCM-41 (50) and Nb-MCM-41 (75) at 200, 250, 300, 350, and 400 °C. Feed rates of *m*-toluidine were set at 4.9 h^{-1} (WHSV) and air (0.021 mol h^{-1} of molecular oxygen), respectively. The results are presented in table 3. The major products were *m*-aminobenzoic acid and *m*-aminobenzaldehyde. *m*-Toluidine conversion increased from 200–250 °C but decreased thereafter. The decrease in conversion above 250 °C was due to coke formation. Although the coke was not analyzed chemically, its formation was confirmed by the charry appearance of the catalysts after the reaction. The mechanism of this reaction is proposed to proceed via an electron abstraction by the niobyl group in the framework as shown below. There is concomitant proton and an electron transfer to the framework niobyl group from *m*-toluidine. The *m*-toluidyl radical reacts with oxygen to yield *m*-toluidyl peroxide radical. This radical in turn abstract hydrogen atom from another *m*-toluidine to yield *m*-toluidyl hydroperoxide. The by-product *m*-toluidyl radical follows the similar reaction route as that of the initial *m*-toluidyl radical. The *m*-toluidyl hydroperoxide decompose to yield *m*-amino benzaldehyde. The hydroxy niobyl species reacts with oxygen to yield hydroxy niobyl peroxide, which in turn abstracts hydrogen atom from *m*-toluidine to yield hydroxy niobyl hydroperoxide. This toluidyl radical put into the same reaction as discussed above. Insertion of oxygen along with C–H bond of *m*-aminobenzaldehyde by the activated oxygen of hydroxy niobyl hydroperoxide gives *m*-aminobenzoic acid the starting niobyl species.

The oxidation over tetravalent niobium in the non-framework niobium oxide may proceed as follows. The niobyl group chemisorbs oxygen to yield a diradical. Hydrogen atom abstraction from *m*-toluidine results in the formation of metal hydroperoxide and metal hydroxide groups. The *m*-toluidine radical follows the sequence of steps as applied to pentavelant framework niobium to yield *m*-aminobenzaldehyde. Insertion of oxygen along with C–H bond of *m*-aminobenzaldehyde using the activated oxygen of metal hydroperoxide yields *m*-aminobenzoic acid. The metal dihydroxide decompose to yield water and the starting niobyl group.

Based on these mechanistic details, it could be said that the increment in conversion at 250 °C might be indicative of high activation energy requirements for the title reaction. Conversion decreased with increase in percent loading of niobium oxide. This variation clearly suggests increase in particle size fusion by tiny niobium oxides of nano dimension with increase in percent loading. Nb-MCM-41 (50) and Nb-MCM-41 (75) showed less conversion than impregnated catalysts. It might be due to high density of niobyl grouping the impregnated catalysts compared to incorporated catalysts. Among the impregnated catalysts the Nb-MCM-41 (1%) showed higher activity than Nb-MCM-41 (2%) and Nb-MCM-41 (3%). It might be due to sintering of tiny niobia particles to bulkier once in Nb-MCM-41 (2%) and Nb-MCM-41 (3%). Among the incorporated catalysts Nb-MCM-41 (50) was found to be more active than the Nb-MCM-41 (75) due to its more density of niobyl groups.

The selectivity to *m*-aminobenzoic acid increased from 200–250 °C, but decreased afterwards. This observation clearly establishes non-availability of activated oxygen due to blocking of active sites by coke. Formation of *m*-aminobenzoic acid by direct oxidation of *m*-aminobenzaldehyde is clearly evident by the reverse trend of *m*-aminobenzaldehyde selectivity to that of *m*-aminobenzoic acid. All the impregnated catalysts showed similar trend to the selectivity of *m*-aminobenzoic acid and the magnitude also remained the same. So, irrespective of the particle size, as discussed above, nearly similar trend in selectivity to *m*-aminobenzoic acid established existence of similar route for the formation of *m*-aminobenzaldehyde.

Table 3
Products distribution of *m*-toluidine oxidation over different catalysts at different reaction temperatures

Catalysts	Temperature (°C)	Conversion (wt %)	Product selectivity (%)		
			m-amino benzoic acid	*m*-amino benzaldehyde	Others
Nb-MCM-41 (1%)	200	29.4	66.8	23.6	10.4
	250	41.1	72.9	25.5	1.6
	300	35.8	61.1	32.8	6.1
	350	28.3	55.5	41.6	2.9
	400	20.1	48.6	45.0	6.4
Nb-MCM-41 (2%)	200	26.8	64.3	25.0	10.7
	250	39.4	68.0	27.0	5.0
	300	33.9	58.9	33.3	7.8
	350	26.6	53.7	39.9	6.4
	400	22.0	46.6	44.6	8.8
Nb-MCM-41 (3%)	200	25.0	60.9	23.8	15.3
	250	37.5	66.5	27.5	6.0
	300	33.0	55.9	34.2	9.9
	350	23.9	51.7	42.5	5.8
	400	18.9	47.5	45.9	6.6
Nb-MCM-41 (50)	200	17.8	55.5	29.0	15.5
	250	31.8	59.8	33.3	6.9
	300	28.5	51.5	36.7	11.8
	350	19.9	47.1	40.9	12.0
	400	16.0	40.7	47.0	12.3
Nb-MCM-41 (75)	200	15.1	51.9	30.1	18.0
	250	25.9	55.5	27.9	16.6
	300	22.3	49.7	37.0	13.3
	350	17.5	45.1	41.2	13.7
	400	14.6	41.0	45.6	13.4

Reaction conditions: 0.3 g of catalyst; WHSV: 4.9 h^{-1} for reactant; air (0.021 mol h^{-1} of molecular oxygen).

The selectivity obtained with isomorphous substituted catalysts was not as high as impregnated catalysts. It might be due to the formation of unidentified products with more selectivity. The selectivity to *m*-aminobenzaldehyde increased with increase in temperature but decreased thereafter for all the catalysts. But the magnitude of selectivity for each temperature was found to be the same for all the catalysts. With isomorphous substituted catalysts the conversion was less but the selectivity to unidentified products was high. The increase in selectivity to unidentified products appeared almost equal to the decrease in selectivity of *m*-aminobenzoic acid. Hence, it indirectly proved that for the unidentified products the precursor might be *m*-aminobenzoic acid. A better possible route might be decarboxylation of *m*-aminobenzoic acid to aniline. It was tested with pure aniline by gas chromatography. The retention time coincided with one of the major components of the unidentified.

3.8. Effect of WHSV

The effect of WHSV was studied over all the catalysts with air as the oxidant. Conversion increased when the WHSV was changed from 3.33–4.95 h^{-1}, but above 4.95 h^{-1} it decreased for all the catalysts (figure 7). For impregnated catalysts the conversion decreased in the following order at WHSV equal to 4.95 h^{-1}: Nb-MCM-41 (1%) > Nb-MCM-41 (2%) > Nb-MCM-41 (3%). For the same WHSV, the isomorphous substituted catalysts showed less activity than impregnated catalysts. The order of activity of isomorphous substituted catalysts is:Nb-MCM-41 (50) > Nb-MCM-41 (75). The increase in conversion at the 4.95 h^{-1} compared to 3.33 h^{-1} illustrates absence of adsorption. But the effect was observed only after 6.66 h^{-1}. The selectivity to *m*-aminobenzaldehyde increased with increase in WHSV over all the catalysts (figure 8). It is attributed to gradual decrease in the oxidation of it to *m*-aminobenzoic acid with increase in WHSV. The selectivity to *m*-aminobenzoic acid increased when the WHSV was increased from 3.33–4.95 h^{-1}. This was followed by a decrease for higher WHSV (figure 9). Based on the selectivity to unidentified products it can be said that the high selectivity of *m*-aminobenzoic acid at 4.95 h^{-1} is due to less conversion of it to any of the unidentified products. As said previously, the selectivity to *m*-aminobenzoic acid

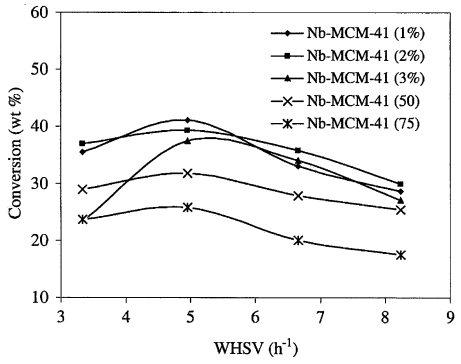

Figure 7. Effect of WHSV on the conversion of *m*-toluidine over Nb-MCM-41 (1%), Nb-MCM-41 (2%), Nb-MCM-41 (3%), Nb-MCM-41 (50), Nb-MCM-41 (75).

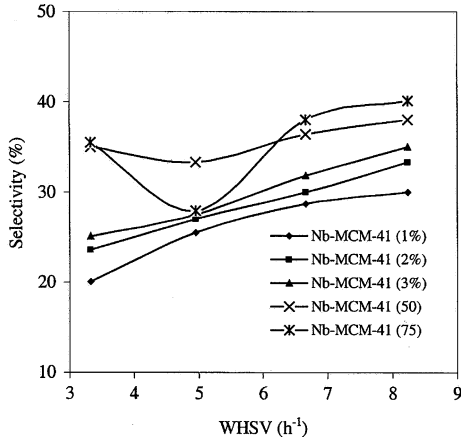

Figure 8. Effect of WHSV on the selectivity of *m*-aminobenzaldehyde over Nb-MCM-41 (1%), Nb-MCM-41 (2%), Nb-MCM-41 (3%), Nb-MCM-41 (50), Nb-MCM-41 (75).

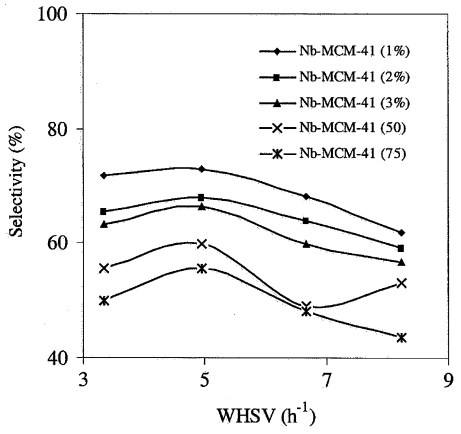

Figure 9. Effect of WHSV on the selectivity of *m*-aminobenzoic acid over Nb-MCM-41 (1%), Nb-MCM-41 (2%), Nb-MCM-41 (3%), Nb-MCM-41 (50), Nb-MCM-41 (75).

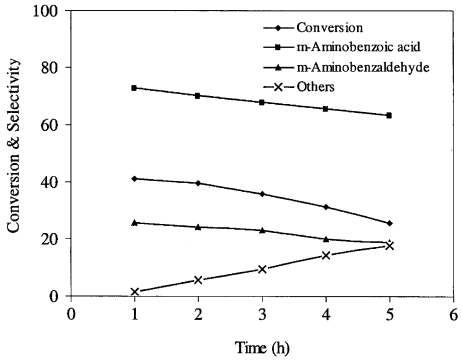

Figure 10. Effect of time on stream on the conversion and products selectivity over Nb-MCM-41 (1%), Nb-MCM-41 (2%), Nb-MCM-41 (3%), Nb-MCM-41 (50), Nb-MCM-41 (75).

is higher over isomorphous substituted catalysts than the impregnated catalysts. It might be due to the formation of unidentified products with more selectivity.

3.9. Effect of time on stream

The effect of time on stream on conversion, selectivity to products and catalytic activity was examined using Nb-MCM-41 (1%), the study was carried out for 5 h. The results of conversion and products selectivity are illustrated in the figure 10. Conversion decreased with increase in stream due to blocking of active sites by coke. The products appeared black but its exact nature was not identified. The selectivity to *m*-aminobenzoic acid decreased with increase in stream but decreased only (2%) at the end of 5 h of stream. Similar trend of decrease was observed for the selectivity to *m*-aminobenzaldehyde. Although it could be expected, increase in selectivity to *m*-aminobenzoic acid due to decrease in selectivity of *m*-aminobenzaldehyde, the decrease in the former may be attributed to increase in its conversion to unidentified products. So, this observation suggests, the active sites that are responsible to decompose *m*-aminobenzoic acid to unidentified products are not blocked by coke formation.

4. Conclusions

From this study, it is concluded that niobium containing MCM-41 can be conveniently used as an eco-friendly catalysts for the oxidation of *m*-toluidine to *m*-aminobenzoic acid. The better exploitability of the catalysts was evident by significant conversion. The impregnated catalysts are found to be more active than isomorphous substituted catalysts. This study is more advantages than liquid phase reaction that use peroxide oxidants. The reaction is continuous and very simple to carry out. Hence, the vapor phase oxidation over niobia catalyst was found to be a successful one even with air as an oxidant. The catalysts were found to be stable even for three cycles of operation. The novelty of this method lies in the fact that the reaction does not use any hazardous peroxide oxidants.

References

[1] J.S. Rafelt and J.H. Clark, Catal. Today 57 (2000) 33.
[2] M. Fetizon and W.J. Thomas, eds., *The Role of Oxygen in Improving Chemical Process*, (The Royal Society of Chemistry, Cambridge, 1993).
[3] G.W. Parshall and S.D. Ittel, *Homogeneous Catalysis, 2nd ed.*, (Wiley, New York, 1992).
[4] D.T. Sawyer, *Oxygen Chemistry*, (Oxford University Press, Oxford, 1991).
[5] D.H.R. Barton, A.E. Martell and D.T. Sawyer, ed., *The Activation, of Dioxygen and Homogeneous Catalytic Oxidation*, (Plenum Press, New York, 1993).
[6] R. Shmidt, D. Akporiye, M. Stocker and O.H. Ellestad, J. Chem. Soc. Chem. Commun. (1992) 1493.
[7] Z.H. Luan, C.F. Cheng, W.Z. Zhou and J. Klinowski, J. Phys. Chem. 99 (1995) 1018.
[8] R.B. Borade and A. Clearfield, Catal. Lett. 32 (1995) 267.
[9] C.F. Cheng and J. Klinowski, J. Chem. Soc. Faraday Trans. 92 (1996) 289.
[10] P.T. Tanev, M. Chibwe and T.J. Pinnavaia, Nature 368 (1994) 321.
[11] A. Corma, M.T. Navarro and J. Perez-Pariente, J. Chem. Soc. Chem. Commun. (1994) 148.
[12] K.M. Reddy, J. Moudrakouski and A. Sayari, J. Chem. Soc. Chem. Commun. (1994) 1059.
[13] Z.Y. Yaun, S.Q. Liu, T.H. Chen, J.Z. Wang and H.X. Li, J. Chem. Soc. Chem. Commun. (1995) 973.
[14] D. Zho and D. Goldfarb, J. Chem. Soc. Chem. Commun. (1995) 875.
[15] S. Vetrivel and A. Pandurangan, J. Mol. Catal. A: Chem. 217 (2004) 165.
[16] N. Ulagappan and C.N.R. Rao, J. Chem. Soc. Chem. Commun. (1996) 1047.
[17] M. Ziolek and I. Nowak, Zeolites 16 (1996) 42.
[18] M. Ziolek, I. Sobczak, I. Nowak, P. Decyk, A. Lewandowska and J. Kujawa, Micro. Meso. Matter. 35–36 (2000) 195.
[19] B. Marler, U. Oberhagemann, S. Vortmann and H. Gies, Micro. Matter. 6 (1997) 375.
[20] S. Vetrivel and A. Pandurangan, Appl. Catal. A: Gen. 264 (2004) 243.
[21] N. He, S. Bao and Q. Xu, Appl. Catal. A: Gen. 69 (1998) 29.
[22] M. Ziolek, I. Sobczak, A. Lewandowska, I. Nowak, P. Decyk, M. Renn and B. Jankowska, Catal. Today 70 (2001) 169.
[23] A.M. Prakash and L. Kevan, J. Am. Chem. Soc. 120 (1998) 13148.
[24] B. Natari, Adv. Catal. 41 (1996) 253.
[25] Y.W. Chen and Y.H. Lu, Ind. Eng. Chem. Res. 38 (1999) 1893.
[26] M. Sugautha and G.V. Subba Rao, J. Solid State Chem. 111 (1994) 33.
[27] Y.M. Kim, D.E. Reardon and P.J. Bray, J. Chem. Phys. 48 (1968) 3396.
[28] D. de A.B. Filho, D.W. Franco, P.P.A. Filho and O.L. Alves, J. Mater. Sci. 33 (1998) 2607.
[29] Z. Sojka, M. Che and E. Giamello, J. Phys. Chem. B 101 (1997) 4831.